



Interlayer modification and single-layer exfoliation of the Ruddlesden-Popper perovskite oxynitride $K_2LaTa_2O_6N$ to improve photocatalytic H_2 evolution activity

Journal:	<i>Journal of Materials Chemistry A</i>
Manuscript ID	TA-ART-03-2023-001387.R1
Article Type:	Paper
Date Submitted by the Author:	25-Mar-2023
Complete List of Authors:	Shiroma, Yuta; Tokyo Kogyo Daigaku, Chemistry Mogi, Hiroto; Tokyo Kogyo Daigaku, Chemistry Mashiko, Takeaki; National Institute for Materials Science Yasuda, Shuhei; Tokyo Institute of Technology, Innovative Research Nishioka, Shunta; Tokyo Institute of Technology, Chemistry Yokoi, Toshiyuki; Tokyo Institute of Technology, Innovative Research Iida, Shintaro; Kumamoto University, Graduate School of Science and Technology Kimoto, Koji; National Institute for Materials Science, Maeda, Kazuhiko; Tokyo Kogyo Daigaku, Chemistry

ARTICLE

Interlayer modification and single-layer exfoliation of the Ruddlesden-Popper perovskite oxynitride $K_2LaTa_2O_6N$ to improve photocatalytic H_2 evolution activity[†]

Received 00th January 20xx,
Accepted 00th January 20xx

DOI: 10.1039/x0xx00000x

Yuta Shiroma,^{a,§} Hiroto Mogi,^{a,§} Takeaki Mashiko,^b Shuhei Yasuda,^{c,#} Shunta Nishioka,^a Toshiyuki Yokoi,^c Shintaro Ida,^d Koji Kimoto,^b Kazuhiko Maeda^{a,e,*}

Modification of the interlayer nanospaces of lamellar solids is an effective means of enhancing the physical properties and chemical functions of such materials. The present work demonstrates the interlayer modification of the layered perovskite oxynitride $K_2LaTa_2O_6N$, a photocatalyst having a ~ 600 nm absorption edge and exhibiting visible-light-driven H_2 evolution activity. This material was subjected to various interlayer modifications, including H^+/K^+ exchange, ethylamine (EA) intercalation and exfoliation with tetra(*n*-butyl)ammonium hydroxide (with subsequent restacking) while maintaining its capacity for visible light absorption. H_2 evolution activity from aqueous methanol with the aid of an optimal amount of a Pt cocatalyst was improved by a factor of approximately 60 following EA intercalation to increase the interlayer spacing of the host material. However, subsequent exfoliation-restacking to yield flocculated nanosheets led to a decrease in activity as compared with the EA-intercalated specimen. The present results indicate that the intercalation of EA provided interlayer nanospaces suitable for Pt cocatalyst loading and so promoted the photocatalytic H_2 evolution reaction, while the restacked nanosheets did not provide space for Pt loading.

Introduction

Two-dimensional materials exhibiting unique structural and electronic properties have many potential applications.¹⁻⁵ In addition, the modification of the interlayer nanospaces in lamellar solids by adding guest molecules or nanoclusters can produce various functional materials, including catalysts, photocatalysts, pigments and protonic conductors.^{4, 6} As an example, expanding the interlayer nanospaces of layered metal oxides is an effective approach for improving the photocatalytic activities of these materials by promoting the reactions of intercalated molecules.^{7, 8} In addition, many lamellar solids, including layered metal oxides, can be exfoliated to produce nanoscale sheets.⁹⁻¹¹ The resulting metal oxide nanosheets comprise anisotropic, nanosized single

crystals having a thickness of 1–2 nm and lateral dimensions ranging from several hundreds of nm to the μm scale. These materials represent useful building blocks for the fabrication of multi-component photosystems in the form of particles¹²⁻¹⁴ or thin films.^{15, 16} In fact, much effort has been devoted to applying oxide-based layered solids as functional materials, and so many approaches to interlayer modification have been developed, including the exfoliation of metal oxides.

Mixed anion compounds have recently received considerable attention as potential functional materials, and the interlayer modification of lamellar mixed anion compounds is of interest.¹⁷⁻¹⁹ As an example, the exfoliation of nitrogen-doped layered $CsCa_2Ta_3O_{10}$ ($CsCa_2Ta_3O_{9.7}N_{0.2}$) as a means of synthesizing a heterogenous photocatalyst has been reported.²⁰ In some cases, phase-pure undoped layered oxynitrides are preferable to their nitrogen-doped analogues because the former exhibit superior visible light absorption and limited formation of anion vacancies due to aliovalent O^{2-}/N^{3-} exchange.²¹ However, the interlayer modification of undoped layered oxynitrides has rarely been reported. This lack of studies can be attributed to the poor stability of undoped layered oxynitrides in the aqueous media²² used for interlayer modification. The limited chemical instability of these materials is a serious challenge, as this instability leads to the loss of nitrogen. This effect eventually lowers the visible light absorption capacity of the compound.

Recently, we found some exceptional cases of chemically stable layered oxynitrides, which include $K_2LaTa_2O_6N$ ²³ and $K_2Ca_2Ta_3O_9N$.²⁴ Ida et al. reported that a three-layer specimen

^a Department of Chemistry, School of Science, Tokyo Institute of Technology, 2-12-1-NE-2 Ookayama, Meguro-ku, Tokyo 152-8550, Japan.

^b Electronic Functional Materials Group, Polymer Materials Unit, National Institute for Materials Science, 1-1 Namiki, Tsukuba, Ibaraki 305-0044, Japan.

^c Nanospace Catalysis Unit, Institute of Innovative Research, Tokyo Institute of Technology, 4259 Nagatsuta-cho, Midori-ku, Yokohama 226-8503, Japan.

^d Institute of Industrial Nanomaterials (IINa), Kumamoto University, 2-39-1 Kurokami, Chuo-ku, Kumamoto 860-8555, Japan.

^e Living Systems Materialogy (LISM) Research Group, International Research Frontiers Initiative (IRFI), Tokyo Institute of Technology, 4259 Nagatsuta-cho, Midori-ku, Yokohama, Kanagawa 226-8502, Japan.

[§] Equal contribution.

[#] Present address: Department of Applied Chemistry, Faculty of Engineering, University of Toyama, 3190 Gofuku, Toyama 930-8555, Japan

[†] Electronic Supplementary Information (ESI) available: [Additional characterization and reaction data]. See DOI: 10.1039/x0xx00000x

of the oxynitride perovskite $\text{Na}_2\text{Ca}_2\text{Ta}_3\text{O}_9\text{N}$ could be exfoliated to produce nanoscale sheets. These sheets exhibited photocatalytic water splitting activity and were also able to transition to a free-standing film.²⁵ The present work demonstrates the interlayer modification and single layer exfoliation of the Ruddlesden-Popper oxynitride $\text{K}_2\text{LaTa}_2\text{O}_6\text{N}$ with the aim of obtaining high photocatalytic activity. $\text{K}_2\text{LaTa}_2\text{O}_6\text{N}$, which has a structure comprising two-layer perovskite blocks, undergoes H^+/K^+ exchange in water while maintaining a suitable degree of visible light absorption.^{23, 26} This material also shows much higher photocatalytic activity than the three-layer analogue because of a longer photogenerated free electron lifetime.²⁴

Therefore, the application of $\text{K}_2\text{LaTa}_2\text{O}_6\text{N}$ to photocatalytic reactions after suitable modification is of interest. The interlayer nanospaces in layered metal oxide photocatalysts are typically employed as reaction sites.^{7, 12, 13, 27-29} However, this technique has rarely been applied to undoped layered oxynitrides. This study confirms that the interlayer modification of the layered oxynitride, $\text{K}_2\text{LaTa}_2\text{O}_6\text{N}$ with a Pt cocatalyst improves photocatalytic activity during visible-light-driven H_2 evolution.

Experimental

Synthesis of layered $\text{K}_2\text{LaTa}_2\text{O}_6\text{N}$

The synthesis was done according to a previously reported procedure with minor modifications.^{23, 26} Briefly, $\text{CsLaTa}_2\text{O}_7$ was first synthesized using a polymerized complex method employing Cs_2CO_3 ($\geq 99.5\%$; Kanto Chemicals Co.), $\text{La}(\text{NO}_3)_3 \cdot 6\text{H}_2\text{O}$ ($\geq 99.0\%$; Kanto Chemicals Co.) and TaCl_5 ($\geq 99.9\%$; Mitsuwa Chemicals Co.) with calcination in air at 1273 K for 2 h. The resulting material was then subjected to a topochemical cation exchange reaction in molten KNO_3 ($\geq 99.0\%$; Wako Pure Chemicals Co.) at 673 K for 48 h to obtain KLaTa_2O_7 . $\text{K}_2\text{LaTa}_2\text{O}_6\text{N}$ was produced by heating the as-prepared KLaTa_2O_7 together with 75 mol% K_2CO_3 ($\geq 99.5\%$; Kanto Chemicals Co.) in a tube furnace at 1173 K for 3 h under a 50 mL min^{-1} flow of gaseous ammonia ($\geq 99.9995\%$; Sumitomo Seika Chemicals Co.).

Intercalation of ethylamine into $\text{K}_2\text{LaTa}_2\text{O}_6\text{N}$

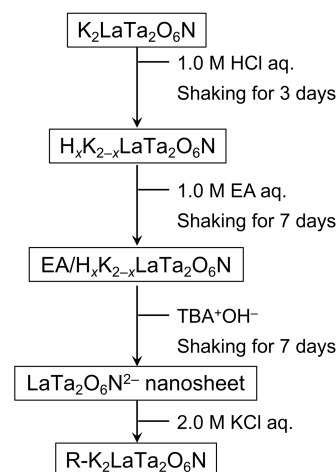
Proton-exchanged $\text{K}_2\text{LaTa}_2\text{O}_6\text{N}$ (referred to hereafter as $\text{H}_x\text{K}_{2-x}\text{LaTa}_2\text{O}_6\text{N}$) was obtained by adding $\text{K}_2\text{LaTa}_2\text{O}_6\text{N}$ (1.0 g) to a 1 M aqueous HCl solution (100 mL) followed by stirring for 3 d. After that, the HCl solution was removed, and the solid product was washed with pure water, separated by centrifugation and dried at room temperature. A portion of the resulting $\text{H}_x\text{K}_{2-x}\text{LaTa}_2\text{O}_6\text{N}$ powder (1.0 g) was subsequently dispersed in a 1.0 M ethylamine (EA; 70 wt% in water; Kanto Chemicals) aqueous solution (100 mL). After agitating this suspension for 7 d at 180 rpm, the solid was collected by centrifugation and then dried overnight at 343 K. The material obtained from this process is referred to herein as $\text{EA}/\text{H}_x\text{K}_{2-x}\text{LaTa}_2\text{O}_6\text{N}$. The intercalation of *n*-alkylamines such as EA into protonated layered perovskite oxides is known to proceed via acid-base interactions.^{11, 30-34} Analyses using solid-state NMR

spectroscopy have also confirmed that the intercalated *n*-alkylamines are present in such materials as the corresponding alkyl ammonium cations.³¹⁻³⁴

Exfoliation of $\text{EA}/\text{H}_x\text{K}_{2-x}\text{LaTa}_2\text{O}_6\text{N}$ and restacking

A quantity of the $\text{EA}/\text{H}_x\text{K}_{2-x}\text{LaTa}_2\text{O}_6\text{N}$ (0.5 g) was added to an aqueous tetra(*n*-butyl)ammonium hydroxide (TBAOH; 40 wt% in water; Aldrich) solution (50 mL) and stirred for 1 week to exfoliate the material into nanosheets. Note that the TBAOH: $\text{EA}/\text{H}_x\text{K}_{2-x}\text{LaTa}_2\text{O}_6\text{N}$ molar ratio in this mixture was 1:1. Any unexfoliated solid was removed by spontaneous precipitation during the first 24 h of this process leaving the supernatant as a nanosheet suspension. Trials, in which the suspended nanosheets were reacted with KCl to induce the formation of a solid, showed that the nanosheet concentration in this dispersion was on the order of 4 g L^{-1} .

Restacked material was obtained by adding a 2.0 M aqueous KCl solution dropwise to the nanosheet suspension. The flocculated solid formed by this addition was then collected by centrifugation and dried in an oven overnight at 333 K. The resulting restacked nanosheets are referred to herein as $\text{R-K}_2\text{LaTa}_2\text{O}_6\text{N}$. The entire materials preparation procedure is depicted in Scheme 1.



Scheme 1. Procedures used for the interlayer modification of $\text{K}_2\text{LaTa}_2\text{O}_6\text{N}$.

Characterization

Powder X-ray diffraction (XRD) patterns were obtained using a Rigaku MiniFlex600 with $\text{Cu K}\alpha$ radiation over the range of 3° – 60° . Solid-state ^{13}C cross-polarization/magic-angle spinning nuclear magnetic resonance (CP/MAS NMR) spectra were acquired with a JEOL ECA-600 spectrometer (14.1 T) equipped with an additional 1 kW power amplifier. The ^{13}C NMR shift was referenced to adamantane as an external standard. The samples were spun at 15 kHz using a 4 mm ZrO_2 rotor under ambient conditions. The textural characteristics of the specimens were assessed by N_2 physisorption at 77 K using a BELSORP-mini II apparatus. Prior to each measurement, the sample was degassed at room temperature overnight under vacuum and then purged with He. Field-emission scanning electron microscopy (FE-SEM) images were obtained using a Hitachi SU9000 instrument. Energy-dispersive X-ray

spectroscopy (EDS) analyses were performed with a Super-X EDS detector system (Thermo Fisher Scientific) to investigate the bulk atomic compositions of K, La, Ta and N. Thermogravimetry (TG) data were obtained using a DTG-60 apparatus (Shimadzu) under a flow of air (50 mL min^{-1}). Al_2O_3 was used as a reference and the rate of heating was 5 K min^{-1} . Atomic force microscopy (AFM) images were acquired with a Nanocute instrument (Hitachi High-Tech) operating in the dynamic mode. Diffuse-reflectance ultraviolet–visible–near-infrared spectroscopy (DRS) data were obtained using a JASCO V-770 spectrophotometer over the 300–700 nm wavelength range. X-ray photoelectron spectroscopy (XPS) was conducted using an ESCA 3400 apparatus (Shimadzu) with Mg $K\alpha$ radiation and the obtained binding energies were corrected by reference to the C 1s peak (285.0 eV). Scanning transmission electron microscopy (STEM) observations were performed in a similar manner to those in previous work³⁵ but with some modifications. The inner and outer detection semiangles of the annular dark field (ADF) detector were 45.8 and 200 mrad, respectively, with an incident probe current of 2–5 pA.

Photocatalytic reactions

Photocatalytic reactions were performed using a closed gas circulation system equipped with a top irradiation type reaction cell.³⁶ In each trial, a 50 mg quantity of the photocatalyst was dispersed in an aqueous methanol solution (10 vol.%, 140 mL) and this suspension was mixed using a magnetic stirring bar throughout the reaction. A 300 W xenon lamp fitted with a cutoff filter was used as the light source ($\lambda > 400 \text{ nm}$). The amount of H_2 generated was determined by a gas chromatograph using Ar as the carrier gas and equipped with a thermal conductivity detector and an MS-5A column. This instrument was directly connected to the closed gas circulation system. The catalyst specimens were loaded with a Pt cocatalyst using an in situ photodeposition method employing $\text{H}_2\text{PtCl}_6 \cdot 6\text{H}_2\text{O}$ (Wako Pure Chemicals) as a precursor.³⁷ The Pt loading was 1 wt% unless otherwise stated.

The apparent quantum yield (AQY) values for the H_2 evolution reaction over the various specimens were obtained using a similar setup but with monochromatic visible light ($\lambda = 420 \text{ nm}$). The AQY was calculated as

$$\text{AQY (\%)} = (2 \times R/I) \times 100,$$

where R and I represent the rate of H_2 evolution and the rate at which incident photons were received, respectively. The total number of incident photons (22.3 mW) was determined using a calibrated silicon photodiode.

Results and discussion

Physicochemical characterization

Figure 1 shows the XRD patterns obtained from the original $\text{K}_2\text{LaTa}_2\text{O}_6\text{N}$ and from the various derivatives. The peak assigned to reflections from 001 planes, which were in the stacking direction of the perovskite layers, was shifted to higher 2θ angles following K^+/H^+ exchange due to the loss of water from the interlayer spaces, as has been previously reported.²³ Treatment of the resulting $\text{H}_x\text{K}_{2-x}\text{LaTa}_2\text{O}_6\text{N}$ with EA

produced a significant low-angle shift of the 001 peak. The interlayer spacing for each sample was calculated from the 001 peak position and this spacing was found to have increased from 12.94 Å in the case of the starting $\text{K}_2\text{LaTa}_2\text{O}_6\text{N}$ to 16.31 Å for the EA/ $\text{H}_x\text{K}_{2-x}\text{LaTa}_2\text{O}_6\text{N}$. Importantly, neither the proton exchange nor the EA treatment significantly affected the positions of peaks related to in-plane reflections (such as the 100 and 110 peaks), as compared with $\text{H}_x\text{K}_{2-x}\text{LaTa}_2\text{O}_6\text{N}$. These results indicate that the interlayer spaces in the $\text{H}_x\text{K}_{2-x}\text{LaTa}_2\text{O}_6\text{N}$ were successfully modified while maintaining the original lamellar structure, which is typical of topochemical reactions. The intercalation of EA was also supported by EDS results. The data in Table 1 demonstrate that the K/Ta and La/Ta ratios were almost unchanged following the reaction of $\text{H}_x\text{K}_{2-x}\text{LaTa}_2\text{O}_6\text{N}$ with EA. CP/MAS NMR spectroscopy confirmed that ammonium cations were intercalated into the $\text{H}_x\text{K}_{2-x}\text{LaTa}_2\text{O}_6\text{N}$, as shown in Fig. S1.

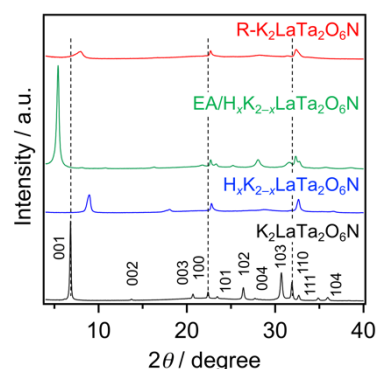


Fig. 1. XRD patterns obtained from the $\text{K}_2\text{LaTa}_2\text{O}_6\text{N}$ and its derivatives.

Table 1. Specific surface areas and elemental compositions of $\text{K}_2\text{LaTa}_2\text{O}_6\text{N}$ and its derivatives

Sample	Specific surface area / $\text{m}^2 \text{g}^{-1}$	Bulk atomic ratio ^a		Surface N/Ta ratio ^b
		K/Ta	La/Ta	
$\text{K}_2\text{LaTa}_2\text{O}_6\text{N}$	5.0	1.01 ± 0.04	0.60 ± 0.04	0.37
$\text{H}_x\text{K}_{2-x}\text{LaTa}_2\text{O}_6\text{N}$	7.4	0.08 ± 0.01	0.52 ± 0.02	0.19
EA/ $\text{H}_x\text{K}_{2-x}\text{LaTa}_2\text{O}_6\text{N}$	16.0	0.10 ± 0.00	0.50 ± 0.01	0.10
R- $\text{K}_2\text{LaTa}_2\text{O}_6\text{N}$	18.4	0.45 ± 0.00	0.51 ± 0.01	0.10
Ideal $\text{K}_2\text{LaTa}_2\text{O}_6\text{N}$	-	1	0.5	-

^a Measured by EDS. ^b Calculated based on the corresponding XPS peak areas. The N 1s XPS peak used for the calculation is attributed to lattice N species.

SEM images of the $\text{K}_2\text{LaTa}_2\text{O}_6\text{N}$ with and without EA intercalation are provided in Fig. 2. Plate-shaped particles reflecting the layered structure of the material can be seen in both specimens, again confirming the successful topochemical reaction. However, the specific surface area, as determined by nitrogen-adsorption at 77 K, was increased from $5.0 \text{ m}^2 \text{g}^{-1}$ in the case of the original $\text{K}_2\text{LaTa}_2\text{O}_6\text{N}$ to $16.0 \text{ m}^2 \text{g}^{-1}$ for the EA/ $\text{H}_x\text{K}_{2-x}\text{LaTa}_2\text{O}_6\text{N}$. The TG data indicated that EA was incorporated in the sample to a level of 8.6 wt% (Fig. S2).

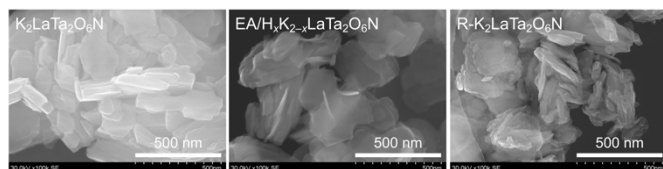


Fig. 2. SEM images of the $K_2LaTa_2O_6N$ and its derivatives.

Exfoliation of the lamellar $K_2LaTa_2O_6N$ to form single-layer sheets was also found to be possible. As shown in Fig. 3a, the reaction of $EA/H_xK_{2-x}LaTa_2O_6N$ with TBAOH resulted in a yellowish colloidal suspension and this suspension was found to be stable for at least 1 month. Figure 3b presents a typical AFM image of the colloidal suspension, in which sheet-like objects having lateral dimensions in the range of 0.1–0.5 μm appear. The height profile obtained from this sample indicates that the thickness of the sheets was approximately 1.3 nm and so was very similar to that of the two-layer perovskite blocks in $K_2LaTa_2O_6N$ as determined from crystallographic data.²³ In addition, the lateral dimensions of the sheets were consistent with those observed in $K_2LaTa_2O_6N$ by SEM (Fig. 2). These results confirm that TBA^+ -exfoliated $LaTa_2O_6N^{2-}$ sheets were successfully prepared, although the material may have contained some residual EA.

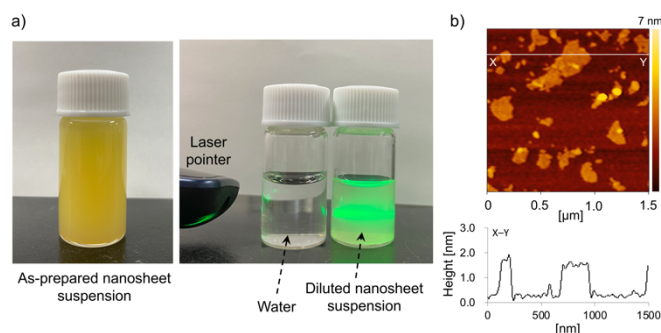


Fig. 3. (a) Digital photographs of the TBA^+ -exfoliated $LaTa_2O_6N^{2-}$ nanosheet colloidal suspension and (b) a typical AFM image and the height profile of a nanosheet.

The addition of KCl to the TBA^+ -exfoliated $LaTa_2O_6N^{2-}$ nanosheet colloidal suspension led to an immediate flocculation of the colloids. The XRD pattern of the flocculated solid (that is, the $R-K_2LaTa_2O_6N$) exhibited weak 001 peaks although the intensity of the in-plane reflection peak remained relatively close to that of the parent $K_2LaTa_2O_6N$ (Fig. 1). These data indicate that the flocculated solid did not retain the long-range order of the layered structure present in the parent material but did keep the original in-plane crystallinity. The same behaviour has been observed in studies with other inorganic layered solids subjected to exfoliation and restacking.^{4, 28} The peak position of the 001 plane in $R-K_2LaTa_2O_6N$ was higher than that of the original $K_2LaTa_2O_6N$, indicating a narrower interlayer. This could be due to the insufficient intercalation of K, which is supported by the EDS results (Table 1). SEM observations also confirmed the formation of a disordered structure in the restacked material (Fig. 2). The specific surface area of the $R-K_2LaTa_2O_6N$ was determined to be $18.4 m^2 g^{-1}$.

As shown in Fig. 4, EA intercalation did not significantly alter the position of the absorption edge of the host $K_2LaTa_2O_6N$, which was located at 580 nm. However, the intensity of the Kubelka-Munk function was decreased following EA intercalation. This result suggests some loss of nitrogen from the $K_2LaTa_2O_6N$, although a quantitative evaluation of the nitrogen content was difficult because the specimen incorporated EA, which also contained nitrogen. The visible light absorption capability was further reduced in the case of the $R-K_2LaTa_2O_6N$. Our group previously demonstrated that layered $K_2LaTa_2O_6N$ shows high (photo)chemical stability in aqueous media. Specifically, the proton-exchange reaction of $K_2LaTa_2O_6N$ in aqueous HCl was found to produce a slight initial reduction in the nitrogen content of the material but no ongoing loss of nitrogen.²³ However, the $K_2LaTa_2O_6N$ could have been damaged by the present multi-step treatment involving proton-exchange, EA intercalation, exfoliation with TBAOH and KCl restacking, resulting in a loss of nitrogen content that lowered the visible light absorption of the material. This possibility is supported by the observation that the bulk N/Ta atomic ratio in the $R-K_2LaTa_2O_6N$ ($N/Ta = 0.38 \pm 0.02$) was lower than that in the layered $K_2LaTa_2O_6N$ ($N/Ta = 0.50 \pm 0.05$).

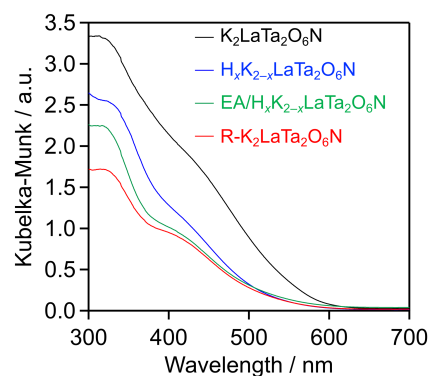


Fig. 4. UV-visible diffuse reflectance spectra of the $K_2LaTa_2O_6N$ and its derivatives.

The surface electronic states of the $K_2LaTa_2O_6N$ and its derivatives were investigated by XPS. As shown in Fig. 5, the K and La peak positions were not changed significantly after proton-exchange, EA intercalation or subsequent restacking, although the K signal was significantly reduced in the case of the $H_xK_{2-x}LaTa_2O_6N$ and the $EA/H_xK_{2-x}LaTa_2O_6N$. In contrast, some changes were evident in the Ta 4f and N 1s spectra. The Ta 4f XPS spectrum of the $K_2LaTa_2O_6N$ contained broad peaks, indicating that Ta species having different oxidation numbers were present in this material (see Fig. S3 for details), as discussed in a previous paper by our group.²⁶ Following proton-exchange, the Ta 4f peak became sharper and showed features typical of Ta^{5+} . A loss of the lattice nitrogen content from the surface was also observed after the proton-exchange (Table 1). It is therefore considered that the nitrogen species bound to the tantalum was removed by the proton-exchange, thereby placing the tantalum in a more oxide-like (more ionic) environment. The intercalation of EA into the $H_xK_{2-x}LaTa_2O_6N$ resulted in a shift of the Ta 4f peak to a lower binding energy

while maintaining the Ta⁵⁺ features. These effects can be ascribed to electronic interactions between the intercalated EA and Ta species in the interlayers. The R-K₂LaTa₂O₆N kept the lower binding energy of the Ta 4f peak even though the majority of the intercalated EA molecules had been removed, as shown in Fig. 1. This result implies that some residual EA molecules remained in the interlayer spaces. Further evidence for this was supplied by the asymmetric peak associated with the 001 reflection of the R-K₂LaTa₂O₆N (Fig. 2). The position of the N 1s peak was also changed, and the change in the binding energy can be explained in the same manner as for the Ta 4f by considering the electron density around Ta atom. It should be noted that the surface N/Ta atomic ratio obtained from the XPS data (N/Ta = 0.10, see Table 1) was much lower than the bulk ratio (N/Ta = 2.83±0.25), again suggesting that EA molecules were intercalated in the bulk H_xK_{2-x}LaTa₂O₆N (see also Fig. S4 and additional discussion in ESI).

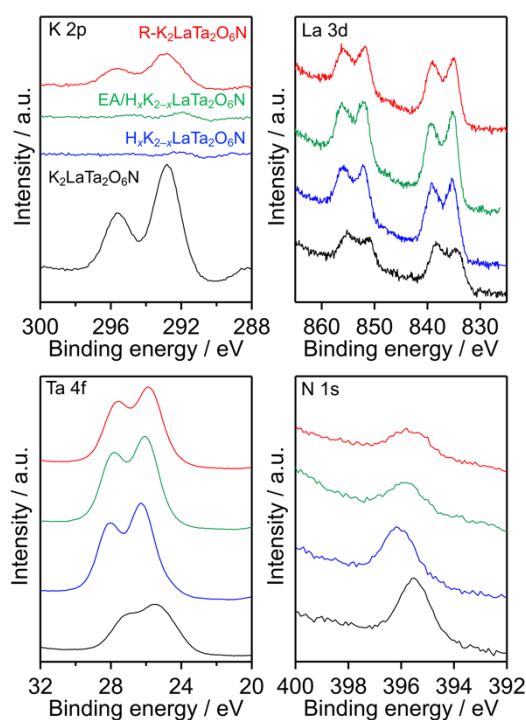


Fig. 5. K 2p, La 3d, Ta 4f and N 1s XPS spectra obtained from the K₂LaTa₂O₆N and its derivatives.

Photocatalytic activities

Trials monitoring H₂ evolution from aqueous methanol solutions were performed using the as-prepared materials under visible light ($\lambda > 400$ nm), and the results are shown in Fig. 6. The layered K₂LaTa₂O₆N and its protonated form both produced H₂ in a stable manner. In addition, the catalytic activity was improved by a factor of approximately 15 following EA intercalation compared with the protonated specimen. The R-K₂LaTa₂O₆N also showed enhanced activity (1.3 $\mu\text{mol h}^{-1}$) as compared with the H_xK_{2-x}LaTa₂O₆N (0.3 $\mu\text{mol h}^{-1}$) but did not outperform the EA/H_xK_{2-x}LaTa₂O₆N (5.4 ± 1.4 $\mu\text{mol h}^{-1}$). No H₂ was produced in the absence of a photocatalyst sample. Overall, these data demonstrate that

suitable interlayer modification of the layered K₂LaTa₂O₆N could improve photocatalytic activity. The EA/H_xK_{2-x}LaTa₂O₆N also showed negligible activity in the absence of methanol (<1 $\mu\text{mol h}^{-1}$), indicating that methanol was exclusively used as the electron donor to facilitate H₂ evolution, rather than the intercalated EA.

The H₂ evolution activity of the EA/H_xK_{2-x}LaTa₂O₆N was found to depend on the Pt loading. As shown in Fig. S5, the H₂ evolution rate was increased with increases in the Pt concentration up to 3 wt%, beyond which the rate decreased. An initial induction period was observed in all cases and was associated with the consumption of photogenerated electrons via reduction of the Pt precursor rather than by water reduction.³⁸ The total amount of H₂ produced from the 3 wt% Pt/EA/H_xK_{2-x}LaTa₂O₆N was approximately 180 μmol , which exceeded the photocatalyst amount (ca. 91 μmol), indicating the catalytic production of H₂. The AQY of the 3 wt% Pt/EA/H_xK_{2-x}LaTa₂O₆N was 2.0% at 420 nm. Although there is a room for improvement of the photocatalytic activity (e.g., by optimizing metal cocatalysts³⁹ and operating conditions⁴⁰), this value is comparable to (or slightly higher than) the AQY of Pt/ZrO₂/TaON (1.7%), one of the most active oxynitride photocatalysts for H₂ evolution.⁴¹ Without Pt deposition, the amount of H₂ evolved was very small (approximately 0.6 μmol over a 10 h reaction), demonstrating that the deposited Pt provided H₂ evolution sites. This enabled to calculate a turnover number for H₂ evolution with respect to Pt to be 23. It should also be noted that increasing the Pt loading from 1 to 3 wt% in trials with the R-K₂LaTa₂O₆N did not increase the H₂ evolution rate (Fig. S6).

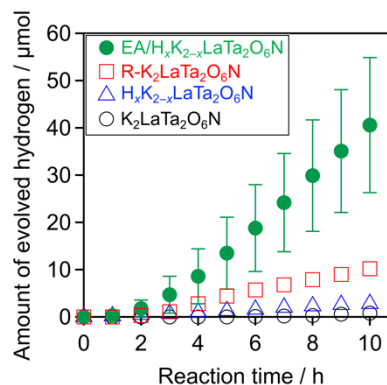


Fig. 6. H₂ evolution over time using the K₂LaTa₂O₆N-based materials under visible light ($\lambda > 400$ nm). Reaction conditions: catalyst, 50 mg (Pt photodeposited in situ); reactant solution, aqueous methanol (10 vol.%, 140 mL); light source, 300 W xenon lamp with a cutoff filter.

Factors affecting photocatalytic activity

The data presented above suggest that the photocatalytic activity of each K₂LaTa₂O₆N derivative during H₂ evolution was strongly dependent on the structure of the material and that the EA-intercalated specimen was the best-performing photocatalyst. Increasing the surface area of a semiconductor photocatalyst may contribute to higher photocatalytic activity because a greater surface area can provide more reaction sites.⁴² As noted, the specific surface area of the EA/H_xK_{2-x}

$x\text{LaTa}_2\text{O}_6\text{N}$ was approximately 3 times that of the $\text{K}_2\text{LaTa}_2\text{O}_6\text{N}$, which qualitatively explains the higher photocatalytic activity of the former. However, the $\text{EA}/\text{H}_x\text{K}_{2-x}\text{LaTa}_2\text{O}_6\text{N}$ and $\text{R-K}_2\text{LaTa}_2\text{O}_6\text{N}$ had similar specific surface areas but different activities. In our previous work, lower-valence Ta species (specifically Ta^{3+}) that were associated with the formation of anionic defects were found to lower the photocatalytic H_2 evolution activity of $\text{H}_x\text{K}_{2-x}\text{LaTa}_2\text{O}_6\text{N}$ by shortening the lifetimes of photogenerated free electrons.²⁶ As shown in Fig. 5, the valence state of the Ta in the $\text{EA}/\text{H}_x\text{K}_{2-x}\text{LaTa}_2\text{O}_6\text{N}$, which was the most active material, was similar to those in the $\text{H}_x\text{K}_{2-x}\text{LaTa}_2\text{O}_6\text{N}$ and $\text{R-K}_2\text{LaTa}_2\text{O}_6\text{N}$. All three specimens exhibited features related almost entirely to Ta^{5+} . Therefore, the relatively high specific surface area and preferable Ta valence state of the $\text{EA}/\text{H}_x\text{K}_{2-x}\text{LaTa}_2\text{O}_6\text{N}$ do not explain the higher photocatalytic activity of this sample.

The XRD pattern obtained from the $\text{EA}/\text{H}_x\text{K}_{2-x}\text{LaTa}_2\text{O}_6\text{N}$ following the reaction showed that the 001 peak position was moved to a higher angle (Fig. 7). This result indicates that the interlayer nanospaces of the $\text{H}_x\text{K}_{2-x}\text{LaTa}_2\text{O}_6\text{N}$, which had been expanded by EA intercalation, were narrowed. This effect was likely due to the removal of the intercalated EA during the reaction. Further evidence for the loss of EA was obtained from the results of ^{13}C CP/MAS NMR and TG analyses (Figs. S1 and S2). Nevertheless, the peak position was still at a lower angle compared with those in the $\text{H}_x\text{K}_{2-x}\text{LaTa}_2\text{O}_6\text{N}$ and $\text{R-K}_2\text{LaTa}_2\text{O}_6\text{N}$ patterns, suggesting that the interlayer spacing in the reacted $\text{EA}/\text{H}_x\text{K}_{2-x}\text{LaTa}_2\text{O}_6\text{N}$ remained wider than in the latter two materials (also see Fig. S7 and additional discussion in ESI). Importantly, no significant changes were identified in the UV-visible DRS data acquired from the sample following the reaction. From this lack of change, it is evident that the capacity of the $\text{H}_x\text{K}_{2-x}\text{LaTa}_2\text{O}_6\text{N}$ for visible light absorption was unaffected (Fig. S7b).

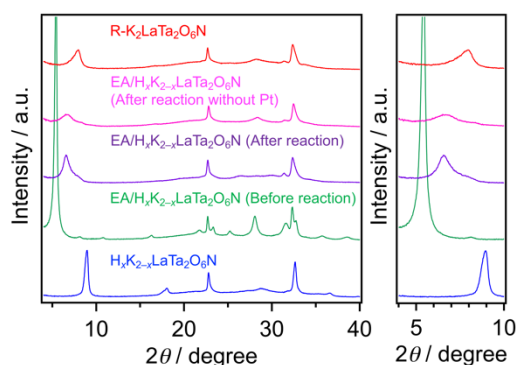


Fig. 7. XRD patterns obtained from the $\text{EA}/\text{H}_x\text{K}_{2-x}\text{LaTa}_2\text{O}_6\text{N}$ before and after the photocatalytic reaction. Data for various reference samples are also shown for comparison.

One possible explanation for the different activities of the present specimens is that the most active material (the $\text{EA}/\text{H}_x\text{K}_{2-x}\text{LaTa}_2\text{O}_6\text{N}$) had expanded interlayer spacing (Fig. 7). This expansion may have promoted redox reactions, as has been reported based on prior work with layered metal oxide photocatalysts.^{12, 13, 27-29} In contrast, no XRD peak shifts were

observed when the same experiment was conducted using the $\text{R-K}_2\text{LaTa}_2\text{O}_6\text{N}$ (Fig. S8). That is, Pt could not be deposited in the interlayer spaces of the $\text{R-K}_2\text{LaTa}_2\text{O}_6\text{N}$.

Fig. 8 presents high-resolution SEM images confirming that the post-reaction $\text{R-K}_2\text{LaTa}_2\text{O}_6\text{N}$ contained a number of Pt deposits having sizes of 2.1 nm on its surfaces (Fig. S9). These Pt deposits were not seen in images of the reacted $\text{EA}/\text{H}_x\text{K}_{2-x}\text{LaTa}_2\text{O}_6\text{N}$. XPS analyses established that the reacted $\text{EA}/\text{H}_x\text{K}_{2-x}\text{LaTa}_2\text{O}_6\text{N}$ and the $\text{R-K}_2\text{LaTa}_2\text{O}_6\text{N}$ both generated Pt signals (Fig. S10) but the surface Pt/Ta atomic ratio was smaller in the former ($\text{Pt}/\text{Ta} = 0.024$) than in the latter ($\text{Pt}/\text{Ta} = 0.046$). The Pt 4f peaks for the $\text{EA}/\text{H}_x\text{K}_{2-x}\text{LaTa}_2\text{O}_6\text{N}$ sample appeared at higher binding energies than those generated by the $\text{R-K}_2\text{LaTa}_2\text{O}_6\text{N}$. This outcome indicates that the Pt species in the former were more cationic than those in the latter and implies that the former Pt species interacted strongly with the $\text{LaTa}_2\text{O}_6\text{N}^{2-}$ layers.¹³ As shown in Fig. S11, the $\text{Pt}/\text{R-K}_2\text{LaTa}_2\text{O}_6\text{N}$ catalysed the H_2 - O_2 consumption reaction while the $\text{Pt}/\text{EA}/\text{H}_x\text{K}_{2-x}\text{LaTa}_2\text{O}_6\text{N}$ did not.

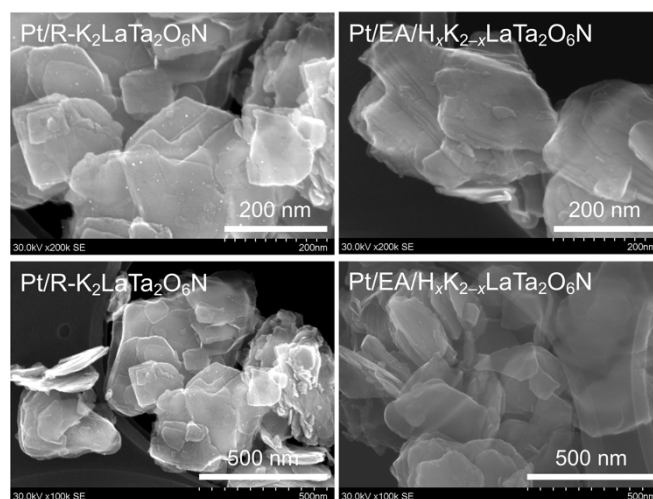


Fig. 8. High-resolution SEM images of the reacted $\text{R-K}_2\text{LaTa}_2\text{O}_6\text{N}$ and $\text{EA}/\text{H}_x\text{K}_{2-x}\text{LaTa}_2\text{O}_6\text{N}$. Pt deposits can be clearly seen as brighter spots in the $\text{Pt}/\text{R-K}_2\text{LaTa}_2\text{O}_6\text{N}$.

From these results, it is apparent that intercalation of Pt species in the interlayers of the $\text{EA}/\text{H}_x\text{K}_{2-x}\text{LaTa}_2\text{O}_6\text{N}$ occurred during the photocatalytic reaction. Additional observations were performed using HAADF/STEM combined with EDS in an attempt to directly observe the intercalated Pt in the material. While clear stripe patterns originating from electron-rich $\text{LaTa}_2\text{O}_6\text{N}^{2-}$ perovskite layers were obtained (Fig. S12), it was not possible to identify any Pt species because of beam-related damage to the sample during the observations and an overlap of the Pt and Ta signals. Nevertheless, it appears that no significant aggregation of Pt species occurred in the $\text{Pt}/\text{EA}/\text{H}_x\text{K}_{2-x}\text{LaTa}_2\text{O}_6\text{N}$. These data help to explain the higher activity of the $\text{Pt}/\text{EA}/\text{H}_x\text{K}_{2-x}\text{LaTa}_2\text{O}_6\text{N}$ during H_2 evolution as compared with the $\text{Pt}/\text{R-K}_2\text{LaTa}_2\text{O}_6\text{N}$.

Interestingly, the $\text{EA}/\text{H}_x\text{K}_{2-x}\text{LaTa}_2\text{O}_6\text{N}$ required a higher Pt loading to achieve peak H_2 evolution performance compared with the $\text{R-K}_2\text{LaTa}_2\text{O}_6\text{N}$ (Figs. S5 and S6). This was the case even though the two materials had almost the same specific surface

areas as determined by nitrogen adsorption experiments. As noted above, a Pt loading of 1 wt% resulted in the majority of the Pt species being introduced into the interlayer nanospaces of the EA/H_xK_{2-x}LaTa₂O₆N (Figs. 8 and S11). However, increasing the Pt loading to 3 wt% caused Pt nanoparticles to deposit on the external surfaces of the specimen (Fig. S13) and, at 5 wt% Pt, the Pt formed larger secondary particles. The need for more Pt in the EA/H_xK_{2-x}LaTa₂O₆N photocatalyst relative to the R-K₂LaTa₂O₆N provides further evidence that the interlayer nanospaces could be utilized as sites for Pt intercalation and H₂ evolution. This was not possible in the R-K₂LaTa₂O₆N, meaning that the EA/H_xK_{2-x}LaTa₂O₆N exhibited higher photocatalytic activity during H₂ evolution.

The sequential photodeposition of Pt onto the EA/H_xK_{2-x}LaTa₂O₆N starting from the interlayers and moving to the external surfaces was thus demonstrated. Evidently, the interlayer nanospaces of the EA/H_xK_{2-x}LaTa₂O₆N had a strong affinity for H₂PtCl₆. It has been reported that 1,2-C₆H₁₀(NH₃)₂²⁺ will react with [PtCl₆]²⁻ to form [PtC₆H₁₀(NH₂)₂Cl₄], most likely as a consequence of a Lewis acid-base interaction.⁴³ A similar Lewis acid-base interaction would be expected to occur between CH₃CH₂NH₃⁺ (i.e., intercalated EA in the EA/H_xK_{2-x}LaTa₂O₆N) and [PtCl₆]²⁻, thereby resulting in the sequential photodeposition of Pt.

Conclusions

An EA-intercalated H_xK_{2-x}LaTa₂O₆N specimen further modified with a Pt cocatalyst was demonstrated to exhibit higher photocatalytic activity for H₂ evolution from an aqueous methanol solution under visible light ($\lambda > 400$ nm) compared with the parent layered material and restacked K₂LaTa₂O₆N nanosheets. Under the optimal conditions, the H₂ evolution activity of the EA/H_xK_{2-x}LaTa₂O₆N was 60 and 18 times higher than those of the H_xK_{2-x}LaTa₂O₆N and R-K₂LaTa₂O₆N, respectively. The expanded interlayer nanospaces in the EA-intercalated material improved loading of the Pt cocatalyst and promoted the photochemical reactions.

Recently, dye-sensitized niobate nanosheets and nanoscrolls have been reported to function as good H₂ evolution photocatalysts capable of functioning under visible light but the low stability of the dye component needs to be addressed.^{14, 44, 45} In contrast to such dye-sensitized oxide systems, oxynitride nanosheets that are already capable of absorbing visible light do not require an additional photosensitizer dye. Thus, the results of this work demonstrate the significant potential of two-dimensional LaTa₂O₆N²⁻ sheets with regard to the construction of visible-light-driven water splitting systems.

Author Contributions

Y.S. performed the majority of the experiments and wrote the manuscript with H.M. and K.M. T.M. and K.K. conducted STEM/EDS analyses. S.Y. and T.Y. conducted NMR and SEM/EDS analyses. S.N. conducted XPS and AQY assessments with Y.S. and analysed the

results. S.I. acquired AFM images. K.M. supervised the project. All authors contributed to the final version of the manuscript.

Conflicts of interest

There are no conflicts to declare.

Acknowledgements

This work was supported by Grants-in-Aid for Scientific Research on the Transformative Research Area (A) "Supra-ceramics" (JP22H05145 and JP22H05148). Part of the research highlighted in this paper was supported by a JSPS Core-to-Core Program (JPJSCCA20200004) and a JST-CREST program (JPMJCR20R2). The crystal structures shown in this work were drawn using VESTA.⁴⁶

Notes and references

1. K. S. Novoselov, A. K. Geim, S. V. Morozov, D. Jiang, Y. Zhang, S. V. Dubonos, I. V. Grigorieva and A. A. Firsov, *Science*, 2004, **306**, 666-669.
2. J. Zhang, Y. Chen and X. Wang, *Energy Environ. Sci.*, 2015, **8**, 3092-3108.
3. A. H. Khan, S. Ghosh, B. Pradhan, A. Dalui, L. K. Shrestha, S. Acharya and K. Ariga, *Bull. Chem. Soc. Jpn.*, 2017, **90**, 627-648.
4. R. Uppuluri, A. Sen Gupta, A. S. Rosas and T. E. Mallouk, *Chem. Soc. Rev.*, 2018, **47**, 2401-2430.
5. K. Maeda and T. E. Mallouk, *Bull. Chem. Soc. Jpn.*, 2019, **92**, 38-54.
6. J. L. Gunjaker, I. Y. Kim, J. M. Lee, Y. K. Jo and S.-J. Hwang, *J. Phys. Chem. C*, 2014, **118**, 3847-3863.
7. Y. Ebina, A. Tanaka, J. N. Kondo and K. Domen, *Chem. Mater.*, 1996, **8**, 2534-2538.
8. J.-H. Choy, H.-C. Lee, H. Jung, H. Kim and H. Boo, *Chem. Mater.*, 2002, **14**, 2486-2491.
9. M. M. J. Treacy, S. B. Rice, A. J. Jacobson and J. T. Lewandowski, *Chem. Mater.*, 1990, **2**, 279-286.
10. T. Sasaki, M. Watanabe, H. Hashizume, H. Yamada and H. Nakazawa, *J. Am. Chem. Soc.*, 1996, **118**, 8329-8335.
11. R. E. Schaak and T. E. Mallouk, *Chem. Mater.*, 2000, **12**, 3427-3434.
12. H. Hata, Y. Kobayashi, V. Bojan, W. J. Youngblood and T. E. Mallouk, *Nano Lett.*, 2008, **8**, 794-799.
13. T. Oshima, D. Lu, O. Ishitani and K. Maeda, *Angew. Chem. Int. Ed.*, 2015, **54**, 2698-2702.
14. T. Oshima, S. Nishioka, Y. Kikuchi, S. Hirai, K. I. Yanagisawa, M. Eguchi, Y. Miseki, T. Yokoi, T. Yui, K. Kimoto, K. Sayama, O. Ishitani, T. E. Mallouk and K. Maeda, *J. Am. Chem. Soc.*, 2020, **142**, 8412-8420.
15. S. W. Keller, S. A. Johnson, E. S. Brigham, E. H. Yonemoto and T. E. Mallouk, *J. Am. Chem. Soc.*, 2002, **117**, 12879-12880.
16. K. Sasaki, K. Matsubara, S. Kawamura, K. Saito, M. Yagi, W. Norimatsu, R. Sasai and T. Yui, *J. Mater. Chem. C*, 2016, **4**, 1476-1481.
17. H. Kageyama, K. Hayashi, K. Maeda, J. P. Attfield, Z. Hiroi, J. M. Rondinelli and K. R. Poeppelmeier, *Nat. Commun.*, 2018, **9**, 772.

18. J. K. Harada, N. Charles, K. R. Poepplmeier and J. M. Rondinelli, *Adv. Mater.*, 2019, **31**, e1805295.
19. K. Maeda, F. Takeiri, G. Kobayashi, S. Matsuishi, H. Ogino, S. Ida, T. Mori, Y. Uchimoto, S. Tanabe, T. Hasegawa, N. Imanaka and H. Kageyama, *Bull. Chem. Soc. Jpn.*, 2022, **95**, 26-37.
20. S. Ida, Y. Okamoto, M. Matsuka, H. Hagiwara and T. Ishihara, *J. Am. Chem. Soc.*, 2012, **134**, 15773-15782.
21. T. Oshima, T. Ichibha, K. S. Qin, K. Muraoka, J. J. M. Vequizo, K. Hibino, R. Kuriki, S. Yamashita, K. Hongo, T. Uchiyama, K. Fujii, D. Lu, R. Maezono, A. Yamakata, H. Kato, K. Kimoto, M. Yashima, Y. Uchimoto, M. Kakihana, O. Ishitani, H. Kageyama and K. Maeda, *Angew. Chem. Int. Ed.*, 2018, **57**, 8154-8158.
22. J. A. Schottenfeld, A. J. Benesi, P. W. Stephens, G. Chen, P. C. Eklund and T. E. Mallouk, *J. Solid State Chem.*, 2005, **178**, 2313-2321.
23. T. Oshima, T. Ichibha, K. Oqmhula, K. Hibino, H. Mogi, S. Yamashita, K. Fujii, Y. Miseki, K. Hongo, D. Lu, R. Maezono, K. Sayama, M. Yashima, K. Kimoto, H. Kato, M. Kakihana, H. Kageyama and K. Maeda, *Angew. Chem. Int. Ed.*, 2020, **59**, 9736-9743.
24. Y. Tang, K. Kato, T. Oshima, H. Mogi, A. Miyoshi, K. Fujii, K. I. Yanagisawa, K. Kimoto, A. Yamakata, M. Yashima and K. Maeda, *Inorg. Chem.*, 2020, **59**, 11122-11128.
25. C.-W. Hsu, T. Ideta, K. Awaya, M. Tsushida, T. Sato, K.-i. Yanagisawa, K. Kimoto, K. Hatakeyama, M. Koinuma and S. Ida, *Chem. Mater.*, 2021, **33**, 6068-6077.
26. H. Mogi, K. Kato, S. Yasuda, T. Kanazawa, A. Miyoshi, S. Nishioka, T. Oshima, Y. Tang, T. Yokoi, S. Nozawa, A. Yamakata and K. Maeda, *Chem. Mater.*, 2021, **33**, 6443-6452.
27. A. Kudo, K. Sayama, A. Tanaka, K. Asakura, K. Domen, K. Maruya and T. Onishi, *J. Catal.*, 1989, **120**, 337-352.
28. Y. Ebina, T. Sasaki, M. Harada and M. Watanabe, *Chem. Mater.*, 2002, **14**, 4390-4395.
29. Y. Ebina, N. Sakai and T. Sasaki, *J. Phys. Chem. B*, 2005, **109**, 17212-17216.
30. J. Gopalakrishnan, S. Uma and V. Bhat, *Chem. Mater.*, 1993, **5**, 132-136.
31. S. Tahara, T. Ichikawa, G. Kajiwarra and Y. Sugahara, *Chem. Mater.*, 2007, **19**, 2352-2358.
32. A. S. Cattaneo, C. Ferrara, A. M. Marculescu, F. Giannici, A. Martorana, P. Mustarelli and C. Tealdi, *Phys. Chem. Chem. Phys.*, 2016, **18**, 21903-21912.
33. I. A. Minich, O. I. Silyukov, V. V. Gak, E. V. Borisov and I. A. Zvereva, *ACS Omega*, 2020, **5**, 8158-8168.
34. S. A. Kurnosenko, V. V. Voytovich, O. I. Silyukov, I. A. Rodionov, S. O. Kirichenko, I. A. Minich, E. N. Malygina, A. D. Khramova and I. A. Zvereva, *Catalysts*, 2021, **11**.
35. H. Wakayama, K. Hibino, K. Fujii, T. Oshima, K. Yanagisawa, Y. Kobayashi, K. Kimoto, M. Yashima and K. Maeda, *Inorg. Chem.*, 2019, **58**, 6161-6166.
36. K. Maeda, M. Higashi, D. Lu, R. Abe and K. Domen, *J. Am. Chem. Soc.*, 2010, **132**, 5858-5868.
37. B. Kraeutler and A. J. Bard, *J. Am. Chem. Soc.*, 1978, **100**, 4317-4318.
38. A. Ishikawa, T. Takata, J. N. Kondo, M. Hara, H. Kobayashi and K. Domen, *J. Am. Chem. Soc.*, 2002, **124**, 13547-13553.
39. M. Hara, J. Nunoshige, T. Takata, J. N. Kondo and K. Domen, *Chem. Commun.*, 2003, DOI: 10.1039/b309935k, 3000.
40. T. Hisatomi, K. Maeda, K. Takanabe, J. Kubota and K. Domen, *J. Phys. Chem. C*, 2009, **113**, 21458-21466.
41. S. S. K. Ma, K. Maeda and K. Domen, *Catal. Sci. Technol.*, 2012, **2**, 818-823.
42. K. Maeda, *J. Photochem. Photobiol., C*, 2011, **12**, 237-268.
43. R. F. Mulagaleev, D. Y. Leshok, A. K. Starkov, A. N. Matsulev and S. D. Kirik, *Journal of Chemistry*, 2017, **2017**, 1-12.
44. S. Nishioka, K. Hojo, L. Xiao, T. Gao, Y. Miseki, S. Yasuda, T. Yokoi, K. Sayama, T. E. Mallouk and K. Maeda, *Sci Adv*, 2022, **8**, eadc9115.
45. C. Davis-Wheeler Chin, P. Fontenot, T. Rostamzadeh, L. J. Treadwell, R. H. Schmehl and J. B. Wiley, *ACS Appl. Energy Mater.*, 2022, **5**, 14687-14700.
46. K. Momma and F. Izumi, *J. Appl. Crystallogr.*, 2011, **44**, 1272-1276.